SHORT TERM Prediction (NOWCASTING) of NET DAILY SEA ICE MOVEMENT IN THE BERING STRAIT WITH A MESOSCALE METEOROLOGICAL NETWORK

by

Thomas L. Kozo, Ph.D.

VANTUNA Research Group

Occidental College

Final Report
Outer Continental Shelf Environmental Assessment Program
Research Unit 519

1984

103

TABLE OF CONTENTS

LIST OF FIGURES

LIST OF TABLES

ABSTRACT

The weather stations at Uelen (Siberia), Bukhta Provideniya (Siberia) and Nome (Alaska) surround the Bering Strait. Surface atmospheric pressure data from this mesoscale triangular station network can be used to calculate hypothetical geostrophic wind velocities in the area of the Strait axis. Net 24 h Strait ice movement has been derived from daily visible and infrared NOAA satellite imagery for the months of November through May from 1974 to 1984. These historical ice motion data and network velocity data have recently been matched to form an empirical 12 h advance forecast (nowcast) prediction scheme for sea ice movement that has all-weather capabilities. In addition, study results have identified three modes of ice movement and two modes of ice immobilization.

The first movement mode is southward requiring a network geostrophic wind of at least 12 ms^{-1} from the northeast and results in transport of ice from the Chukchi Sea to the Bering Sea. The second mode is northward ice movement from the Bering to the Chukchi Sea during weak northerly or southerly winds, driven mainly by a pre-existing north flowing ocean current. The third and least common mode is northward ice movement under the combined influence of a geostrophic wind from the southwest and the north flowing ocean current.

The first immobilization mode is an apparent balance between the wind stress from the north and water stress from the south, plus internal ice stresses resulting in O net movement but existing for time periods generally less than one week. The second and least common immobilization mode was discovered during cases where the model erroneously predicted large ice

movement southward through the Strait. Instead, satellite imagery showed large double solid sea ice arches had formed in the Strait. One arch reached from the Chukchi Peninsula (Cape Dezhneva) to the Diomede Islands and one reached from the Diomede Islands to the Seward Peninsula (Cape Wales). These arches remained intact under 26 ms^{-1} geostrophic winds from the northeast and resulted in O net ice movement through the Strait for up to four weeks.

1. Introduction

The prospect of oil development in the northern Bering Sea has led to recent studies of northward and southward sea ice movement through the Bering Strait (Fig. 1). This movement in the months from November to May can be quite extensive and be intimately connected to destructive interactions with sea ice in the St. Lawrence Island (Shapiro and Burns, 1975a; Sodhi, 1977) and Norton Sound vicinities (Stringer and Hufford, 1982). One example of these interactions can be seen in Fig. 2 (bottom) where southward ice movement below the Strait is related to westward movement of ice out of the Sound (Stringer and Hufford, 1982). Figure 2 (top) shows the atmospheric pressure field determined by pattern recognition techniques (Hufford and Scheidt, 1984), most often associated with this interaction. Another example can be seen in Fig. 3 (bottom) where northward ice movement into the Bering Strait and eastward ice movement into the Sound occur simultaneously (Stringer and Hufford, 1982). Fig. 3 (top) again shows the atmospheric pressure pattern most often associated with this phenomenon (Hufford and Scheidt, 1984). Note that this last case is a type of relaxation with wind forcing at a minimum.

Sequential Landsat (NASA) and DAPP (U.S. Air Force) imagery was used as early as March 1973 to construct displacement vectors for ice floes moving through the Bering Strait (Shapiro and Burns, 1975b). They showed an apparent relationship between southward ice movement and northerly winds at Cape Wales on the western tip of the Seward Peninsula (Fig. 1). This movement occurred despite average yearly northward water transport (Coachman et al., 1975). Ray and Dupre (1981) also noted that the National Weather

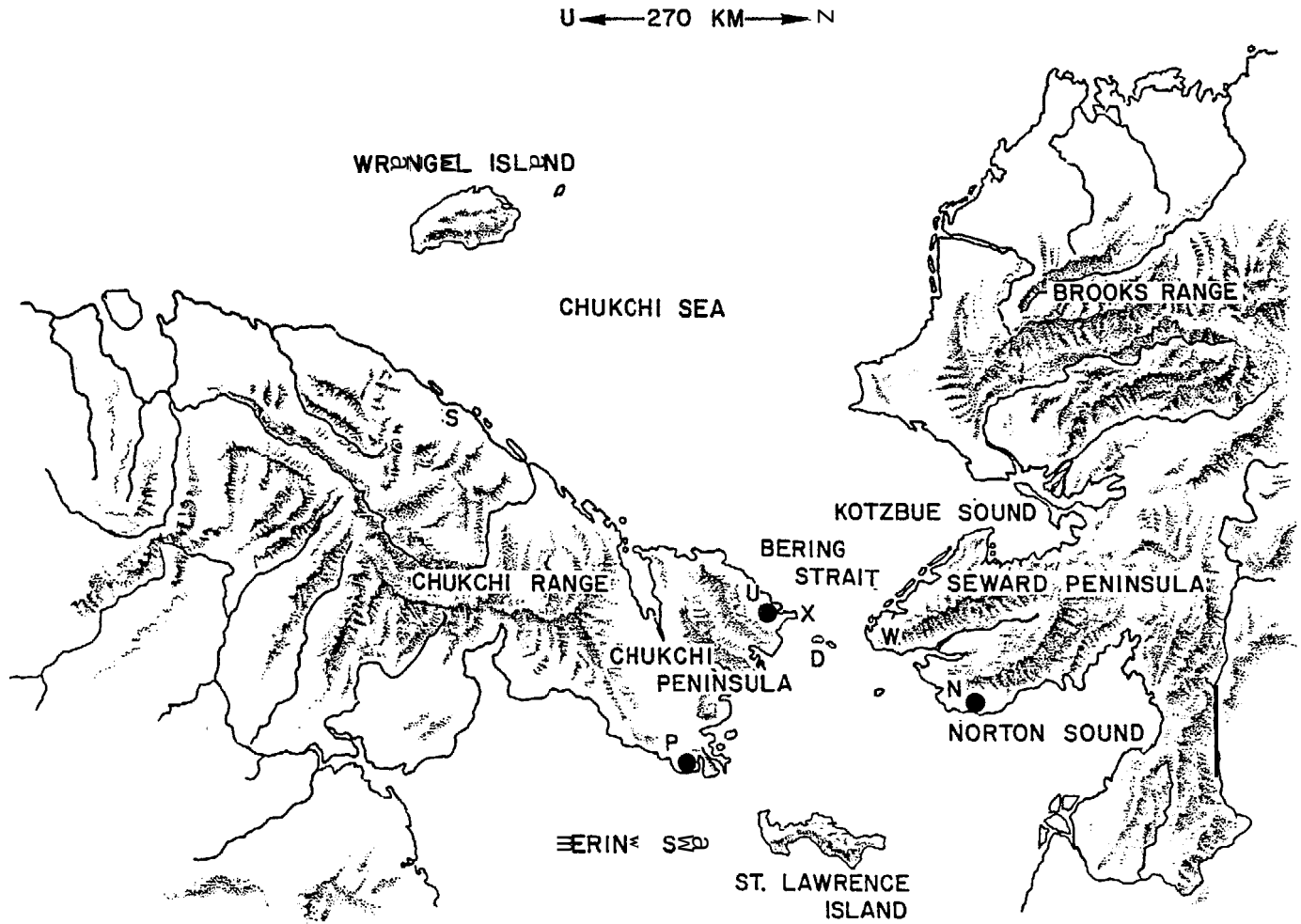

Fig 1 The surface pressure station network P-U-N covering the Bering Strait region. P is Bukhta Provideniya, U is Uelen (both in Siberia) and N is Nome, Alaska. The Diomede Islands (D) are in the center of the Strait, Cape Schmidt S) is below Wrangel Island, and Cape Wales (W) and Cape Dezhneva (X) are on the tips of the Seward and Chukchi Peninsulas respectively. Mountain axes are shaded for emphasis.

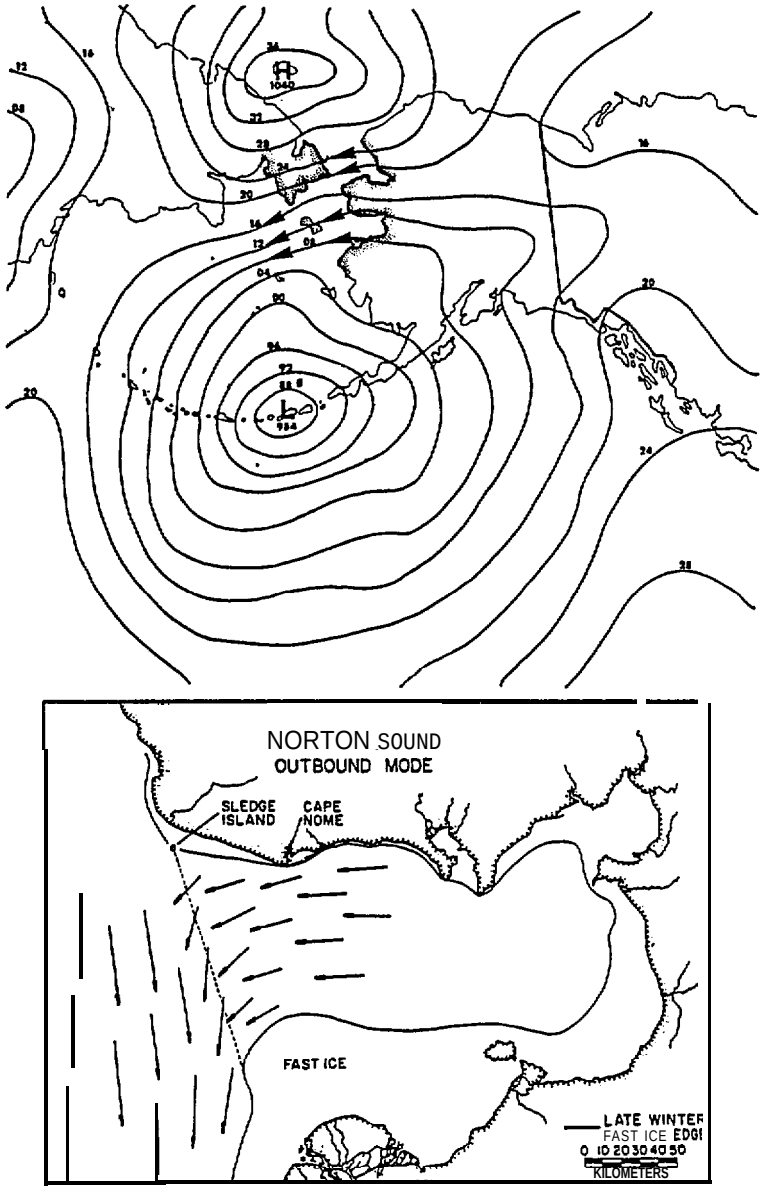

Fig. 2. The atmospheric pressure field (top) determined by pattern recognition techniques (Hufford 1984) that is associated with southward ice movement below the Strait and westward movement (bottom) of ice out of Norton Sound (Stringer and Hufford, 1982). Arrows on isobars (top) indicate wind direction in the Strait area.

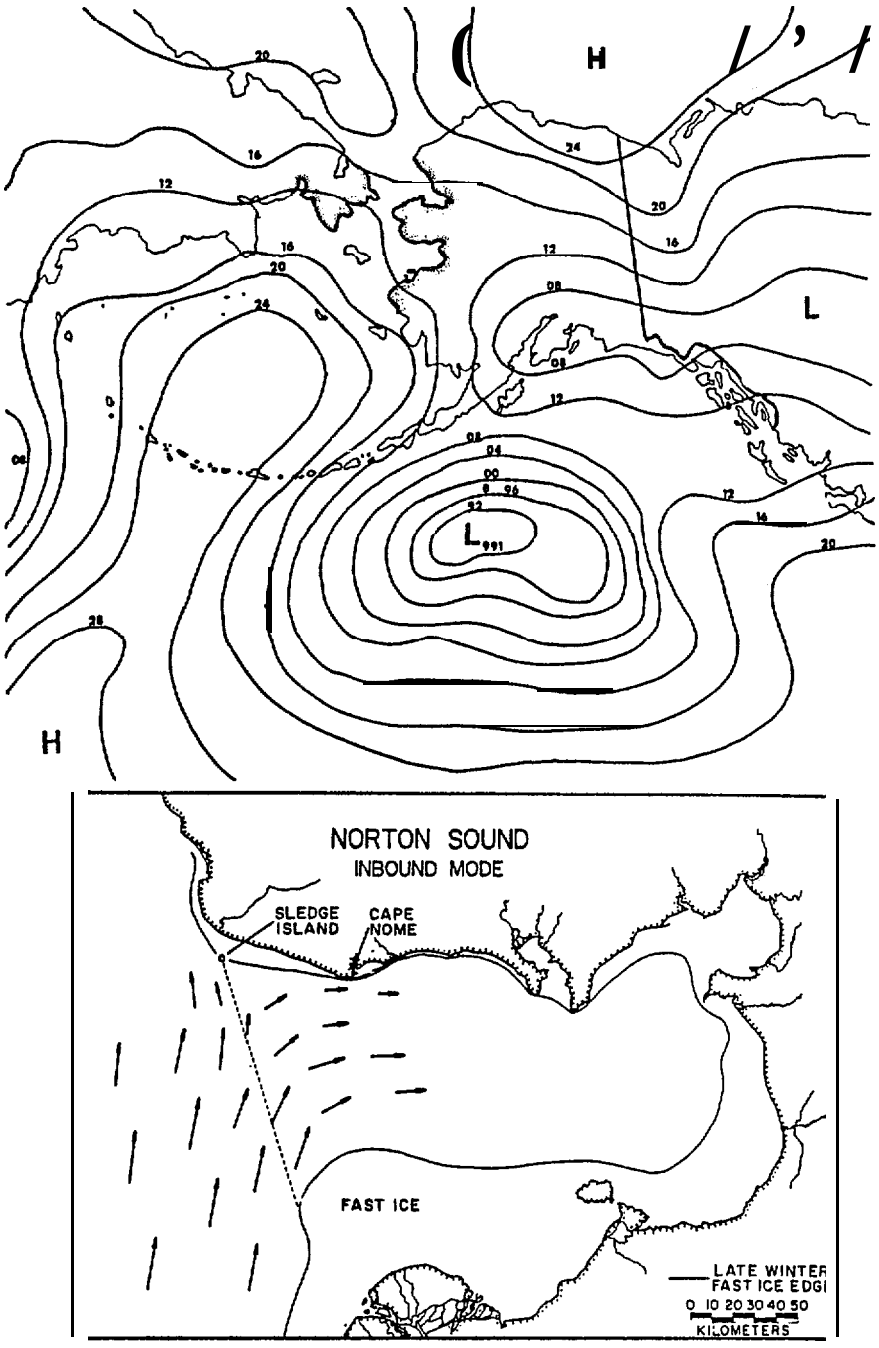

Fig. 3. The "relaxed" atmospheric pressure field (top) determined by pattern recognition techniques (Hufford, 1984) that results in northward ice movement into the Strait and eastward movement (bottom) of ice into Norton Sound (Stringer and Hufford, 1982).

Service surface synoptic charts apparently explained alternating southward and northward sea ice movement in the Bering Strait region deduced from February 1976 sequential Landsat imagery. Large-scale sea ice fracture resulting in southward flow through the Bering Strait (ice breakout) has been studied (Reimer et al., 1979). They modeled the Strait as a two-dimensional chute and computed the necessary load required to fracture and push ice. An atmospheric pressure difference from Cape Schmidt (Siberia) to Nome Alaska, (see Fig. l) exceeding 20 mb was related to ice breakout events in the winters of 1975 and 1976. This was an interesting study, but the geostrophic wind which can be related to the direction of stress application is perpendicular to the pressure gradient, not parallel. It will be shown below, on examination of a greater data sample, that a whole suite of wind directions often produced by pressure differences less than 20 mb from Cape Schmidt to Nome can shove ice south through the Strait.

The tools for short range, less than 24 h prediction (nowcasting [Browning, 1982]) of sea ice movement through the Bering Strait existed, but two preliminary tasks were still to be performed. First, an appropriate atmospheric pressure network encompassing the Bering Strait with at least three World Meteorological Organization (WMO) reporting stations had to be found for computation of geostrophic wind velocities. Second, long records of continuous north and south sea ice motion had to be compiled from available satellite imagery to determine precursor characteristics. The three network stations found were Uelen (U, Siberia), Provideniya (P, Siberia) and Nome (N, Alaska) (Fig. 1). The continuous records of sea ice motion were computed from 11 years of daily visible and infrared NOAA 3-8 satellite photographs. Table 1 is a listing of some Strait sea ice movement events documented from these photographs.

TABLE 1

EXAMPLES OF PAST SEA ICE MOVEMENT EVENTS THROUGH THE BERING STRAIT

Documented by Satellite Imagery

Courtesy of Dr. Bill Stringer, University of Alaska, Geophysical Institute

Year	Month	South Days	North Days
1974	April	8-12	
1976	February	5-12, 22-25	26-28
	April	17-20	
	Nov.-Dee.	29-2	
	December	10-11	3-9
1977	February	10-12	
	March	1-2, 25-26	
	April	2-3, 9-12	
1978	March	4-7, 27-28	21-25
	April	7-9	
1979	February	26-27	16-24
	April	9-11	
1980	February	**20-22**	1-3 (March)
	April	6-7, 18	
	December	7-13, 24-25, 30-31	19-21
1981	February	13, 16-19	4
	December	5-7	13
1982	March	14-15, 19-20	2-4
	April	12-13, 27	18-21
1983	January	1-4, 7-8, 16-19	18-15
	February	17-22	
	March	9-15, 22-24, 16-30	
	April	4-6	

2. Study Area

The Bering Strait's oceanic cross section is roughly 85 km x 50 m and its annual average transport is ∿ 1 Sv to the north, attributed to higher sea level in the Bering Sea than in the Arctic Ocean (Coachman and Aagaard, 1981). This relatively small annual northward transport would be five times greater if not for wind induced flow reversals to the south occurring two to three times per month and lasting six to 12 days (Kovacs and Sodhi, 1981). Daily mean transport can reach 3.1 Sv (Coachman and Aagaard, 1981) to the north which implies currents up to 70 cms^{-1}, given the above cross sectional area. Current velocities of this magnitude are indications that oceanic flow driven north or south tend to be funneled (see Fig. 1) and accelerated on entering the Strait (Coachman et al., 1975).

The same funneling applies to arctic winds in the Strait which tend to flow around rather than over topography (Kozo, 1984). The Chukchi Peninsula has small mountain range axes setting north to east while the Seward Peninsula has small mountain range axes setting north to west (Fig. 1). The elevations are at least equal to 600 m which Dickey (1961) has shown are sufficient to redirect and accelerate air flow during winter conditions.

During the course of this study, it became apparent that ice moved north and south through the Strait as if on a conveyor belt (Kozo and Tucker, 1974) for a suite of computed wind velocity vectors. Therefore, relating ice movement thresholds to a wind velocity component parallel to an assumed strait axis orientation would simplify development of a prediction nomogram. However, determining the precise axis orientation for ice transit thresholds was not easy. In addition to water and wind stresses, the ice movement

threshold values would be affected by interplay of internal ice stresses, land boundary effects and fast (immobile shore-attached) ice zone boundary effects. Even the fixed land boundaries (Fig. 1) present a problem. The Chukchi Peninsula coastlines above and below the Strait are oriented 135° and 45° from the north, respectively. The Seward Peninsula coastlines above and below the Strait are oriented 55° and 145° from the north, respectively. The perpendicular to the line of minimal distance (Cape Dezhneva to Cape Wales, Fig. 1) across the Strait is 31° from the north. Evidently there were several choices of axis orientation. For the purposes of this paper, the internal ice stresses and fast ice edge effects were neglected and the Strait axis orientation was chosen to be 40° from the north. This angle represents a perpendicular to the line from Cape Schmidt to Nome (Fig. 1). In this way, comparisons can be made with earlier work by Reimer et al. (1979) where a positive pressure difference (20 mb) between Cape Schmidt and Nome was related to ice breakout into the Bering Sea.

3. Data

a. Surface atmospheric pressure and temperature

Barometric pressure data, reduced to sea level, and temperature data are taken simultaneously from a three station weather network and used to compute a hypothetical geostrophic wind for the Bering Strait. The three stations are part of the global weather network and transmit real-time data to the National Meteorological Center (NMC). They are Uelen (66″10′N, 169°50'W), Bukhta Provideniya (64°26′N, 173°14'W), and Nome (64°30'N, 165°24'W) (see Fig. 1). The accuracies of these pressure and temperature data from Nome, a first order weather station, are better than ±.25 mb and ±1°C, respectively.

The two Russian stations are assumed to be within these limits also.

b. Geostrophic wind data

These data were computed from the pressure and temperature data provided by the three above weather stations. The atmospheric flow was assumed to be in geostrophic balance (l):

$$f(k \times V) + \frac{\nabla p}{\rho} = 0 \qquad (1)$$

The first term is the Coriolis force, and the second is the pressure gradient force. f is the Coriolis parameter (1.321×10^{-4} sec^{-1} at 65°N), k is the vertical unit vector, V is the velocity vector, ∇p is the gradient of the atmospheric pressure, and ρ is the air density. Using the above station grid (triangle in Fig. 1) and noting that pressure can be represented as a function of latitude (y) and longitude (x) on a plane surface, the following set of equations:

$$\begin{aligned} P_N(x,y) &= ax_N + by_N + c \\ P_U(x,y) &= ax_U + by_u + c \\ P_P(x,y) &= ax_p + by_p + c \end{aligned} \qquad (2)$$

are generated, where the subscripts N, U, and P denote Nome, Uelen and Provideniya, respectively. Pressure (P) data is broadcast by each station and relative positions of each station are known on an x,y grid. Cramer's rule can be applied to (2) to solve for unknowns a, b and c. Since $\partial P/\partial x = a$ and $\partial P/\partial y = b$, the pressure gradient (VP) can be computed. The geostrophic velocity can now be calculated from (1) since f is known and p for dry air can be estimated from station temperatures.

Station errors of ±1°C (see above) in temperature can cause errors of .34% in the velocity magnitude since they affect p estimates. Station errors in pressure of ±.25 mb can cause maximum speed errors ±1.4 ms^{-1} and direction errors greater than ±15° for wind speeds below 3 ms^{-1}. Therefore, at wind speed ≦3 ms^{-1}, wind directions should not be considered significant.

The main objective of this study was to create a nomogram for predicting ice movement in the Bering Strait from computed geostrophic wind velocities. The "true" geostrophic winds, therefore, are not as important as geostrophic wind values derived from consistent data sources that comprise the triangular network surrounding the Strait. Successful use of mesoscale network computed geostrophic winds and their increased resolution and predictive capabilities over synoptic networks in the Arctic has been documented by Kozo (1980, 1984).

c. Satellite imagery

The imagery used in this study came primarily from visible and infrared NOAA 3-8 VHRR (very high resolution radiometer) satellite photographs. The infrared imagery was utilized primarily during the months of December, January and February when daylight was minimal. In order to minimize errors due to the earth's curvature, the scale was taken from the closest land mass. The net ice motion in a 24 h period was measured directly by tracking identifiable floes or indirectly by measuring the change in open water extent south or north of the Diomede Islands (Fig. 1). A minimum of two consecutive days of imagery is necessary to document a displacement. The error for a typical two-day sequence is estimated at ±5 km. However, for sequences greater than two days, the error reduces significantly.

From November 1974 to May 1984, close to 40% of the total observation days during the ice-covered months (November through May) have been obscured due to cloud related undercast. Therefore, the nomogram produced from these empirical observations has not included a large percentage of the total possible ice movement data. However, the product and technique outlined below based on the remaining 60% of the data, if representative, will be an all-weather, undercast independent, predictive tool.

4. Results with Discussion

a. Sea ice injections

The available satellite imagery (1974 to 1984) has shown many episodes of extensive south and north sea ice movement analagous to ice injections through the Strait typically lasting five to seven days. There have been 39 cases of southward injections into the Bering Sea and 19 cases of northward injections into the Chukchi Sea where the total ice input approximately equaled the areal extent of St. Lawrence Island (Fig. 1, SLI). Of the 39 southward cases, 17 had an input more than twice the area of SLI. For the 18 northward cases, only seven occurred with an input of double SLI's area.

b. Advantages of the mesoscale atmospheric pressure network

Fig. 4 shows the advantage of a mesoscale atmospheric pressure network (MAPN) for predicting ice movement through the Bering Strait over that of the NMC surface pressure analysis. The NMC surface isobaric analysis for 21 April 1982, 1200 Greenwich Mean Time (GMT) gives no indication of a strong southwesterly wind. In addition, the surface wind directions at Uelen (U),

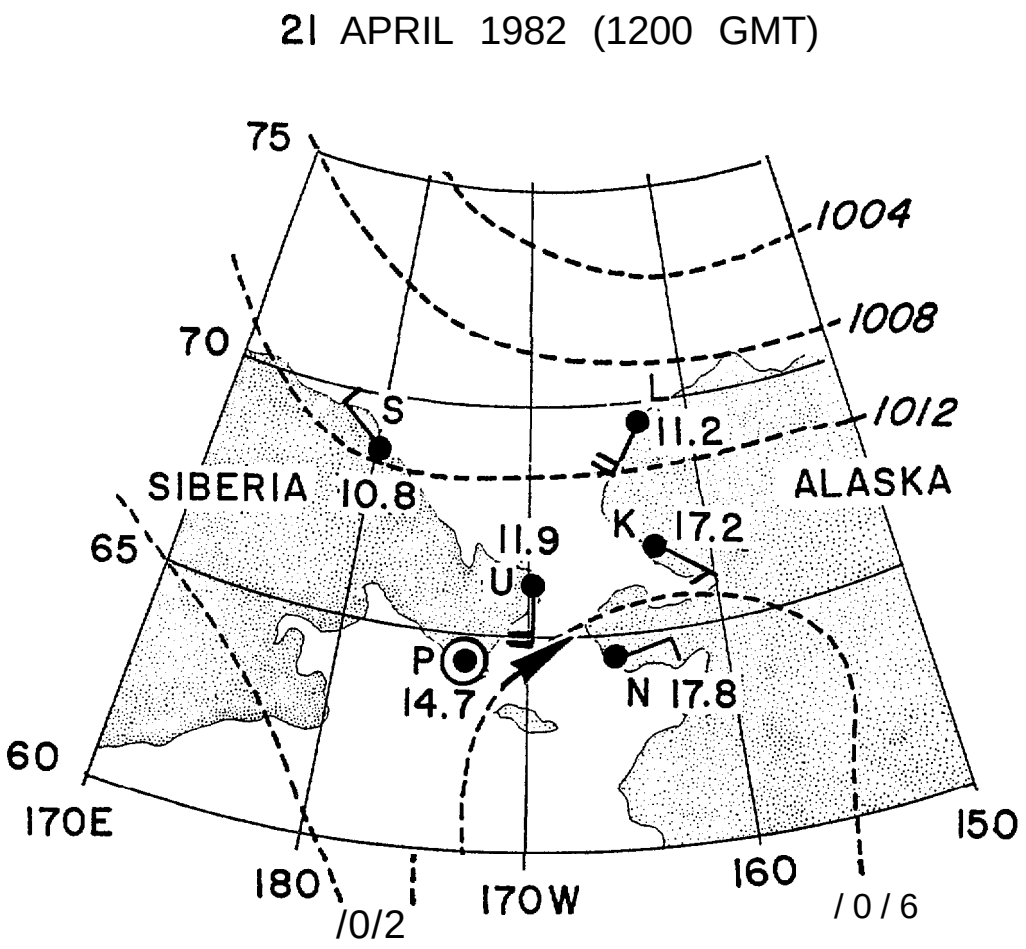

Fig. 4. An example of the lack of detail on an NMC surface isobaric analysis (dashed lines in rob). The mesoscale network (Provideniya [P], Uelen [U], and Nome [N]) shows a V_G (see arrow) of 12.4 ins-l from 248°. The surface wind speeds at designated station locations are ∿ 5 ms^{-1} for each perpendicular flag, ∿ 2.5 ms^{-1} for slant flags (i.e. Kotzebue [K]) and ∿ 0 for a circle (i.e. P). Other stations shown are Point Lay (L) and Cape Schmidt (S). The sea ice in the Strait area moved 15 km to the north.

Provideniya (P), and Nome (N) are all different (Fig. 4). However, the surface wind velocity (~ 10 ms^{-1} from 180°) at Uelen may offer a clue to the eventual ice push direction. Satellite imagery indicated that ice in the Strait moved 15 km north (±5 km) for this day. The MAPN calculated geostrophic wind (V_G) was 12.4 ms^{-1} from 248° which fits the observed net motion.

Fig. 5 is a case demonstrating the advantage of the MAPN over both pattern recognition and NMC synoptic analysis. A type of relaxation mode has existed for four days (as in Fig. 3, top) which denotes probable northward ice movement. However, the MAPN calculated geostrophic wind velocity indicates that the "brakes" are being applied to northward sea ice movement. The 1200 GMT, 25 March 1978 V_G was 11.0 ms^{-1} from 75° and the average V_G for the next 12 h period was 12.4 ms^{-1} from 68.4°. The net ice movement for 25 March was 6 km south (±5 km). The surface winds surrounding the Strait (Fig. 5) appear to be less than 5 ms^{-1}, but their northerly direction may also be a clue to the direction of wind push.

The effects of orography are striking, even with a well defined surface pressure pattern as demonstrated on April 5, 1983 (Fig. 6). The "dog's breakfast" of surface wind directions at P, U and N are evidence that previous attempts to correlate these local winds with ice movement or ocean current direction in their vicinity met with limited success (Coachman et al., 1975 and Reimer et al., 1979). The MAPN calculated V_G was 23 ms^{-1} from 56.8°, again agreeing with the satellite determined large net ice movement of 50 km (±5 km) south in one day.

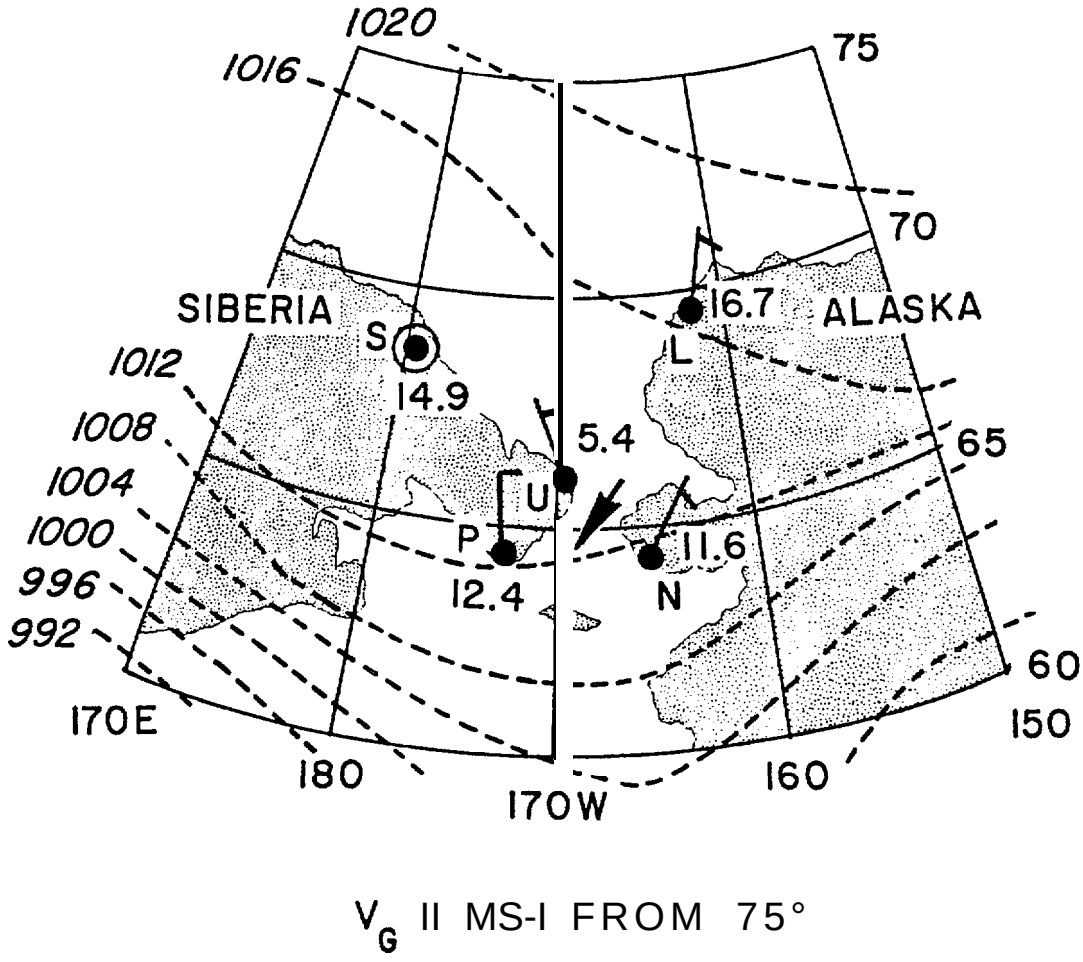

Fig. 5. An example of the advantages of the network P-U-N analysis over both pattern recognition and NMC surface isobaric analysis (dashed lines in mb). Despite an apparent "relaxation", the 1200 GMT network analysis shows a V_G (see arrow) of 11.0 ms^{-1} from 75°. The station and flag designations are as in Fig. 4. The sea ice in the Strait area moved 6 km to the south.

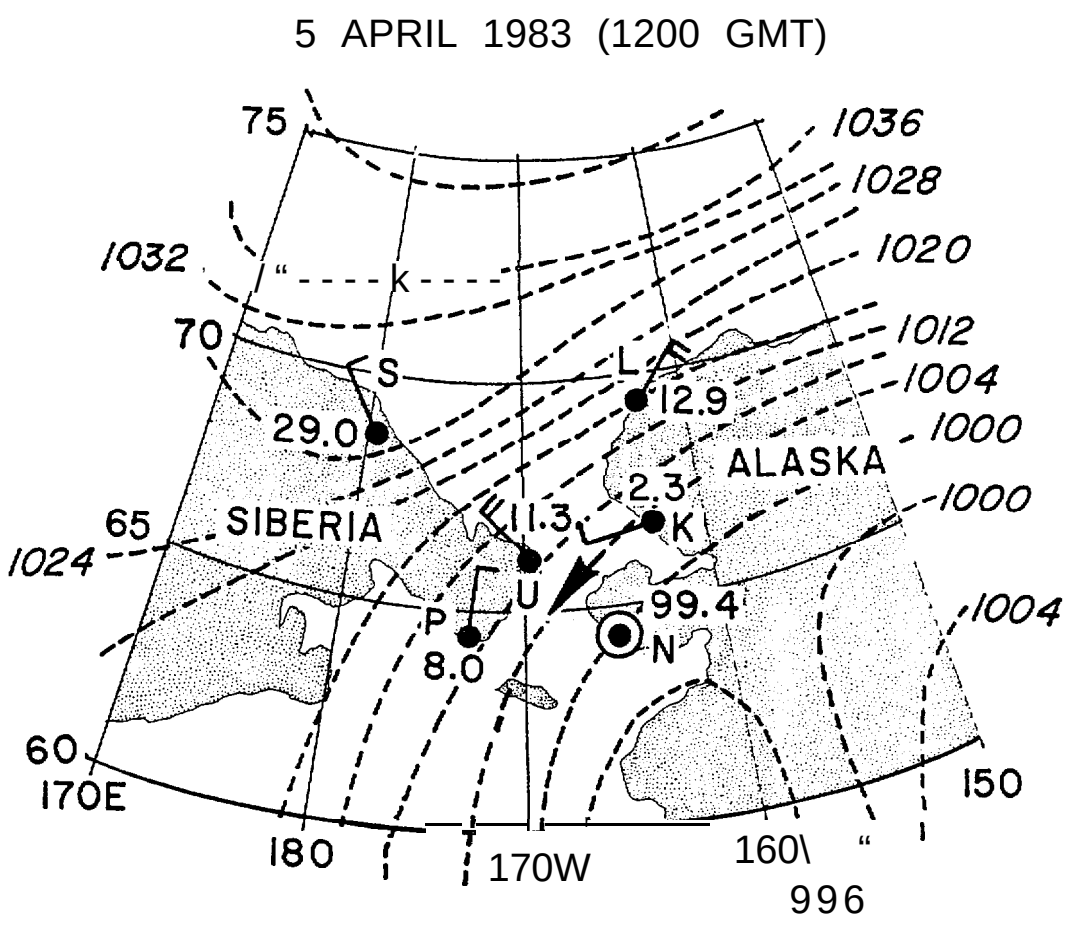

Fig. 6. An example of the effects of orography on the surface wind directions despite a well defined isobaric pattern (dashed lines in rob). The P-U-N network analysis shows V_G (see arrow) of 23 ms^{-1} from 56.8°. The station and flag designations are as in Fig. 4. The Nome (N) and Kotzebue (K) winds would give no clue that the sea ice in the Strait moved 50 km to the south during this day.

c. Implications for oceanic transport mechanisms

During the course of this nowcasting study, several minor discoveries were made. One of them provides evidence that previous conclusions concerning the persistent northward oceanic transport through the Strait may have to be reexamined. Coachman and Aagaard (1981) have stated that the basic driving force for this transport is a yet unexplained higher mean sea level in the Bering Sea than in the Arctic Ocean. They also state that short (several day) increases in northward flow volume have two causes. The first is a compensatory acceleration of flow following a wind induced southward transport event. After the driving wind subsides, ocean transport continues south for a short time raising the water level in the St. Lawrence Island-Norton Sound area (Fig. 1), resulting in an enhanced sea level slope down to the north. This creates a large increase in transport to the north with a one day time lag. The second cause was the development of a strong low-pressure center (counterclockwise rotation) in the western Bering Sea, south and west of the Strait with isobars oriented north-south through the Strait. In this case, southwesterly winds push water onto the relatively shallow northern Bering Sea shelf, again enhancing sea level slope down to the north.

It must be noted that current data were not measured coincident with the time period discussed below, however net sea ice movement was measured. This movement, in cases of weak synoptic winds, will indicate surface current velocities. The 00 GMT, 11 May 1984 NMC synoptic chart (Fig. 7) shows a weak high to the southwest of the Strait promoting slight off-shelf water movement in the Bering Sea. In addition, the atmospheric pressure field shows a 12 mb decrease in sea level pressure from the southwestern Bering to the

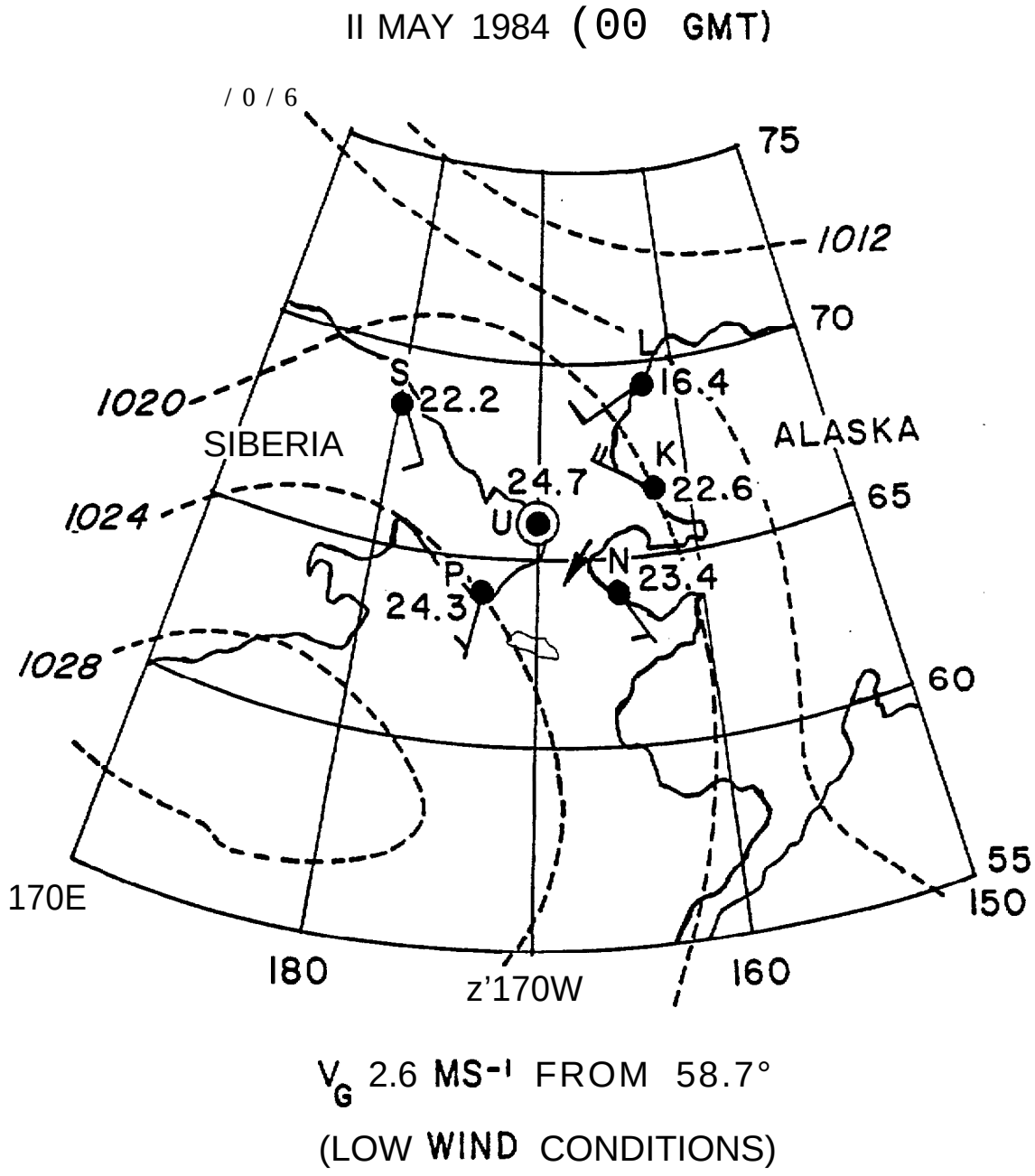

Fig. 7. A section of an NMC surface pressure analysis that indicates weak surface winds and no apparent reasons for sea level in the Bering to be higher than that of the Chukchi. The net sea ice movement calculated with P-U-N data was 18 km to the north for a V_G (see arrow) of 2.6 ins-l from 58.7°.

northeastern Chukchi Sea. Both effects would tend to make the sea level in the Bering lower than in the Arctic Ocean, promoting southward current flow since it is opposite to the condition mentioned by Coachman and Aagaard (1981). This synoptic condition persisted on May 11 and was imbedded in a period from May 4 to May 15, 1984 of relatively weak synoptic winds. The net sea ice movement on May 11 was 18 km (±5 km) north and followed a day of almost no motion. This event was evidence that northward current flow occurs without southwesterly wind forcing or a sea level slope down to the north. The same event also showed that accelerated flow can occur without a sea level imbalance caused by a previous northerly wind. The MAPN calculated V_G (Fig. 7) was a low 2.6 ins-l from 58.7° (see errors for speeds < 3 ms^{-1} in Section 3b). The synoptic charts for the entire day showed no winds strong or persistent enough to produce the recorded ice movement. This event took place under relaxed conditions similar to those depicted in Fig. 3 which were found by pattern recognition techniques to be representative of northward ice movement.

There is ample evidence that all the mechanisms listed above (Coachman and Aagaard, 1981) are sufficient conditions for northward oceanic transport, however, this example shows that they are not necessary conditions for this type of transport. The recent ocean modeling work of Liu and Leendertse (1982) has shown a net residual circulation in the Strait area due to only the tides and density field (baroclinic mode) with current amplitudes of ~ 10 cms^{-1}. Their current characteristics match the data of Drury et al. (1981). Based on this new modeling effort, weather map analysis such as Fig. 7 and net ice motion data, a northward flowing current driven only by tidal residuals and the ocean density distribution must exist in the Strait without the need for additional wind push or sea level differences.

d. **Constructing the sea ice movement prediction nomogram**

Sea ice satellite images from November 1974 to May 1984 have been examined and compared to simultaneous MAPN computed V_G's to produce an empirical 12-hour advance forecast (nowcast) nomogram. Table 2 gives the dates and mode categories for some of the sea ice movement events used in constructing the nomogram (Fig. 8). The Greek and Latin letters from Table 2 are positioned in Fig. 8 to represent a MAPN computed V_G (direction and speed as independent variables). The directions indicated are those from which the wind is blowing. The small center circle (Fig. 8) represents V_G's with speeds less than 3 ms^{-1}. Due to the errors mentioned in Section 3 and the minimal effects on ice motion at these low wind speeds, V_G's within this circle should be considered as ~ 0 winds. V_{40} (see Table 1 for sign) represents the V_G component parallel to the assumed Strait axis, 40° from north. This axis is indicated by ice movement direction arrows (Fig. 8) that meet in the Force Balance Zone, one of five zones defined by wind speed ranges along the 40 axis. These zones and the nomogram technique have characterized three modes of ice motion and two modes of ice immobilization in the Strait, Four predictable modes will be described below in conjunction with Fig. 8 and Table 2. The fifth mode, though not predictable, was a discovery of this procedure and will be discussed in Section 4g below.

Mode 1 covers two zones and represents wind-forced sea ice movement into the Bering Sea which initially at least must offset a northward flowing ocean current. To get measurable ice movement into the Bering, V_{40} must exceed 11.5 ms^{-1} (Fig. 8, Table 2). The ICE INTO BERING ZONE has 11.5 ms^{-1} $< V_{40} \leq 16.5$ ms^{-1} and produces net ice movement of < 20 km $(day)^{-1}$. The ICE INTO BERING > 20 km $(day)^{-1}$ (ZONE) has $V_{40} > 16.5$ ms^{-1}. The latter zone

TABLE 2

SELECTED SEA ICE MOVEMENT EVENTS FOR THE BERING STRAIT

PLOTTED IN FIG. 8.

A. Referring to Fig. 8, V_{40} ❑ V_G speed component to Strait axis 40° from north.

B. If V_G direction	> 310° or < 130°	> 0
	= 310° or = 130°	$'_{40}$ = 0
	130° < V_G < 310°	< 0

c. No estimates of turning angle (directional difference between V_G and V surface) were made since orographic effects such as channeling and blockage were very apparent and no concomitant long term data base exists.

Mode 1. Into Bering Sea (wind-forced)

a. > 20 km $(day)^{-1}$ (V_{40} > 16.5 ms^{-1})

Events: Y(14,15 Apr 82), Z(14,15 Mar 82)

ɣ(13 May 78, λ(18 May 77), Δ(11 Feb 84)

ϕ(6,7 Mar 78), Ψ(27 Dec 76)**

**Ψ also represents the average value needed to reverse the ocean current, at 10 m off the bottom in the Bering Strait, from north to south for all three cases in Dec 76 (Coachman and Aagaard, 1981) during total ice cover

b. < 20 km $(day)^{-1}$, (11.5 ms^{-1} < V_{40} ≦ 16.5 in^{s-1})

Events: U(18 Feb 84), X(19 Feb 83), N(12 May 81)

V(22 Feb 76), W(19 Feb 76), M(11 May 81)

TABLE 2. (continued)

Mode 2. Into Chukchi Sea (ocean current forced, wind influence minor)

a. > 20 km $(day)^{-1}$, (-7.5 ins-l < $V_{40} \leqq$ O ms^{-1})***, weak winds in current direction

***If Vs_{urface} is ∿ 60% of V_{40}, then (7.5 ins-l x .6) = 4.5 ins-l or WMO equivalent of a gentle breeze

Events: A(10,11 Feb 79), B(16,17 Feb 79), C(1,2 Feb 76)
D(27,28 Feb 76), E(20,21 Mar 78), F(2,3 Mar 82)

b. < 20 km $(day)^{-1}$, (0 ms^{-1} < $V_{40} \leqq$ 7.5 ins-l), weak winds oppose current direction

Events: K(9 Apr 82), R(27 Apr 82), T(3 May 84)
Q(24 Feb 79), 1(23 Jan 82)

Mode 3. Into Chukchi Sea (ocean current and wind influence as major forces)

a. > 20 km $(day)^{-1}$, ($V_{40} \leqq$ - 7.5 ms^{-1})

Events: G(8 Apr 82), 0(6 Feb 82), Π(4 Feb 82)
ω(24 Feb 82)

b. no cases < 20 km $(day)^{-1}$ for $V_{40} \leqq$ - 7.5 ms^{-1}

Mode 4. First immobilization mode (no movement through Strait)

a. (7.5 ins-l < $V_{40} \leqq$ 11.5 ins-l), wind and water stresses in balance

Events: J(23,24 Mar 82), S(2 May 77), H(30 Mar 82)
L(20,21 Apr 81), 0(11 Apr 78), P(2 Apr 78)

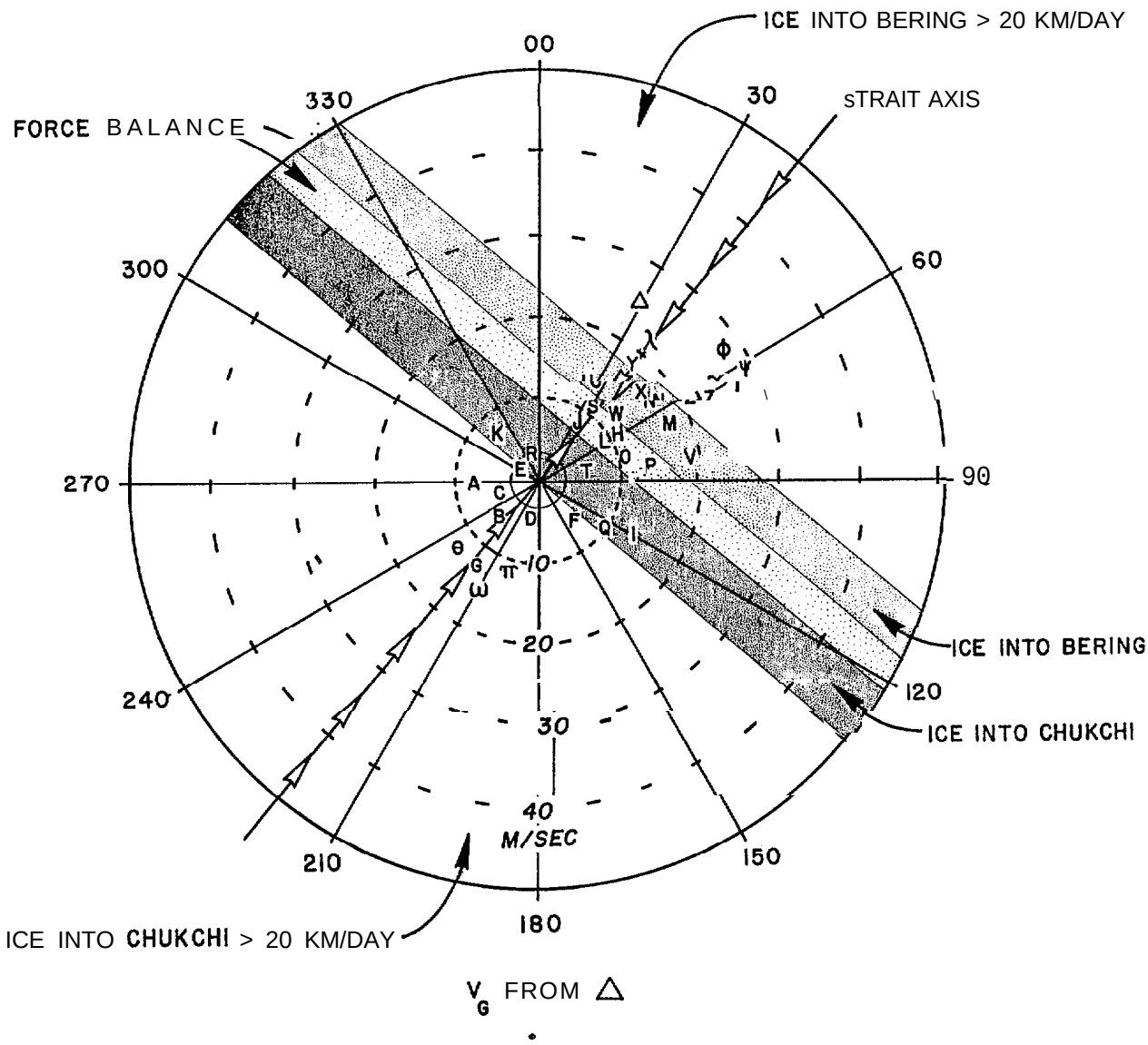

Fig. 8. The Bering Strait sea ice movement prediction nomogram with Greek and Latin letters representing sample MAPN computed $\bar{V}_G$'s used in its construction (see Table 2). The Strait axis is 40° from the north and has ice movement arrows meeting in the Force Balance Zone. The center solid circle is the ≦ 3 ms^{-1} wind speed zone and it represents direction uncertainties >15°.

conditions, if persisting for five days, would represent a total sea ice injection into the Bering Sea approximately equal to double the area of St, Lawrence Island (Fig. 1).

Included in these zone conditions were three cases (December 11, 20, and 27, 1976) during total ice cover when the ocean current at 10 m from the bottom switched from north to south in the Bering Strait (Coachman and Aagaard, 1981). Y (Fig. 8) represent the average MAPN computed V_G during these three cases (29 ms^{-1} from 61°). The 27 December 1976 event was the only one with clear satellite imagery. It showed net southward ice movement through the Strait of 25 km.

Mode 2 (Table 2) includes two zones of northward sea ice movement into the Chukchi Sea and represents an ocean current dominated mode with only minor wind influence. The ICE INTO CHUKCHI > 20 km(day)$^{-1}$ ZONE (Fig. 8), for -7.5 ms^{-1} $\leq V_{40} \leq$ 0 ms^{-1}, exists due to a pre-existing northward flowing ocean current. This current (see Section 4c) appears to be a combination of residual contributions from the Bering Sea tide and density fields (Liu and Leendertse, 1982) and a semi-permanent downward sea level slope from the Bering toward the Chukchi (Coachman and Aagaard, 1981). This also corresponds to the relaxed wind field case (Fig. 3, top) of Hufford and Scheidt (1984) that results in northward ice motion adjacent to Norton Sound (Fig. 3, bottom). Sea ice injections into the Chukchi Sea equal to double the area of St. Lawrence Island (Fig. 1) will occur in five days. The ICE INTO CHUKCHI ZONE (Fig. 8) with 0 ms^{-1} $\leq V_{40} \leq$ 7.5 ms^{-1} has a weak wind regime that opposes the northward flowing ocean current reducing the net sea ice movement to < 20 km (day)$^{-1}$.

Mode 3 does not occur as frequently as the previous two. It (Table 2) includes only one zone of northward sea ice movement into the Chukchi Sea

(Fig. 8) and represents a mode under the combined influence of both the wind and ocean current. Mode 3 is always within the ICE INTO CHUKCHI > 20 km(day)$^{-1}$ ZONE (Fig. 8) since the wind and water stress are in the same direction. However, Mode 3 has sometimes produced less net movement than the ∿ 0 wind push cases in Mode 2. The Mode 2 case represents a localized Strait area ocean current push on the sea ice canopy from below. The Mode 3 case is a combination of the localized ocean current push and a large area wind stress pushing the entire sea ice canopy in the northern Bering Sea. This indicates that opposing internal and boundary stresses within the ice may play a larger role in the Mode 3 case.

Mode 4 is one of 0 net ice movement, usually lasting less than one week, and it includes the Force Balance Zone with 7.5 ms^{-1}<V_{40}≦11.5 ,s^{-1} ,he primary force balance in the Strait area is between the wind stress pushing ice south and the water stress pushing ice north. Again, internal ice stresses and shore-fast ice boundary effects must play a role, but they are beyond the scope of this study. A check on the relative magnitudes of the opposing surface wind stress (τ_a) and water stress (τ_w) can be made as follows using values typical of the Strait conditions:

$$\tau_a = \rho_a C_a (u_a \cdot r_a)^2 \quad (3)$$

$$\tau_w = \rho_w C_w U^2_w) \quad (4)$$

where pa ≡ density of dry air at -20°C ∿ 1.4 kgm^{-3}

C_a ≡ 10 m drag coefficient for air/water in the Bering Sea area ∿ 3x10 ,3 (Walter et al., 1984)

U_a ❑ average wind speed in the Force Balance Zone ∿ 10 ms^{-1}

r_a ≡ ratio of surface wind speed (10 m) to the calculated geostrophic wind ∿ .6 ms ,1 (Albright, 1980) for Arctic

conditions . Note: Albright used a high resolution surface pressure grid and multiyear data base to derive his r_a"

$\rho_w \equiv$ density of water at O*C $\sim 1x10^3$ kgm^{-3}

$C_w \equiv$ 2 m drag coefficient for ice/water in the Bering Sea area $\sim 16x10^{-3}$ (Pease and Overland, 1984)

$u_w \equiv$ typical current speed due to residual contributions from the tide and density distribution in the Bering Strait area $\sim .1$ ms^{-1} (Liu and Leendertse, 1982)

comparing (3) and (4) after inserting the above values:

$$\tau_a \square 1.4 \times 3x10^{-3}x(10x.6)^2 = .15 \text{ N}_m{}^{-2}$$

$$\tau_w \equiv 1x10^3 \text{ X } 16x10^{-3}(.1)^2 = .16 \text{ N}_m{}^{-2}$$

These values are quite comparable for the opposing stresses and add credibility to the nomogram design.

e. Using the nomogram

The users of this nomogram would follow a simple procedure provided that they have access to weather data transmissions similar to that of NMC. Simultaneous surface pressure and temperature data from Uelen, Provideniya, and Nome (Fig. 1) for 00 and 1200 GMT should be available to the user less than three hours after recording at the respective stations. These data (P_N, $_U$, P_p) can be input into the system of equations (2) in Section 3b to solve for ∇p. Air density (p) can be approximated using an average temperature from the three stations and the equation of state for dry air, $p = P(RT)^{-1}$. P is the standard sea level atmospheric pressure (1013.3 rob), R is the gas constant and T is the absolute temperature. The solution for VP, p and ultimately V (V_G in our case) can be obtained from (1) using any programmable hand calculator. The V_G for 00 and 1200 GMT are combined to obtain an

average velocity ($\bar{V}_G$). Once $\bar{V}_G$ is known, the two necessary independent variables, speed (radius vector) and direction (vectorial angle), can be plotted on polar coordinate graph paper (for best resolution) with the nomograms five wind speed zones and '40 axis superimposed. For example, using data from Fig. 6, P_N = 999.4 mb, P_p = 1008.0 mb, P_U = 1011.3 mb, and an average temperature of -5°C (not shown in Fig. 6), V_G = 23 ms'^{1} from 56.8°. Plotting this value on Fig. 9 (X, bottom) and finding the V_{40} component by drawing a perpendicular from the V_{40} axis to X shows that the nomogram predicts net ice movement > 20 km (day)$^{-1}$ to the south. The actual net ice movement was 50 km south.

f. Testing the nomogram technique

(1) NOAA satellite imagery

Fig. 9 (bottom) represents the nomogram base chart as constructed from data in Fig. 8. In this case, a time period having 23 consecutive days (April 6-28, 1982) free of major undercast was chosen to test the accuracy of the MAPN and nomogram predictions. The numbers 6-28 are April dates and represent the positions of the 00 and 1200 GMT mean V_G's on those days. If the wind direction changes by more than 90° in 12 h, and/or the change would reverse the direction of ice motion, no prediction would be made. If any of the three network stations failed to report at either the 000 or 1200 GMT time periods, then the closest available simultaneous time period was used for the average V_G. Fig. 9 (top) shows the net sea ice direction and movement in km for the corresponding days. Remembering that the error bounds on the imagery were ±5 km and the V_g's were ±1.4 ms^{-1}, the nomogram technique failed in only three cases.

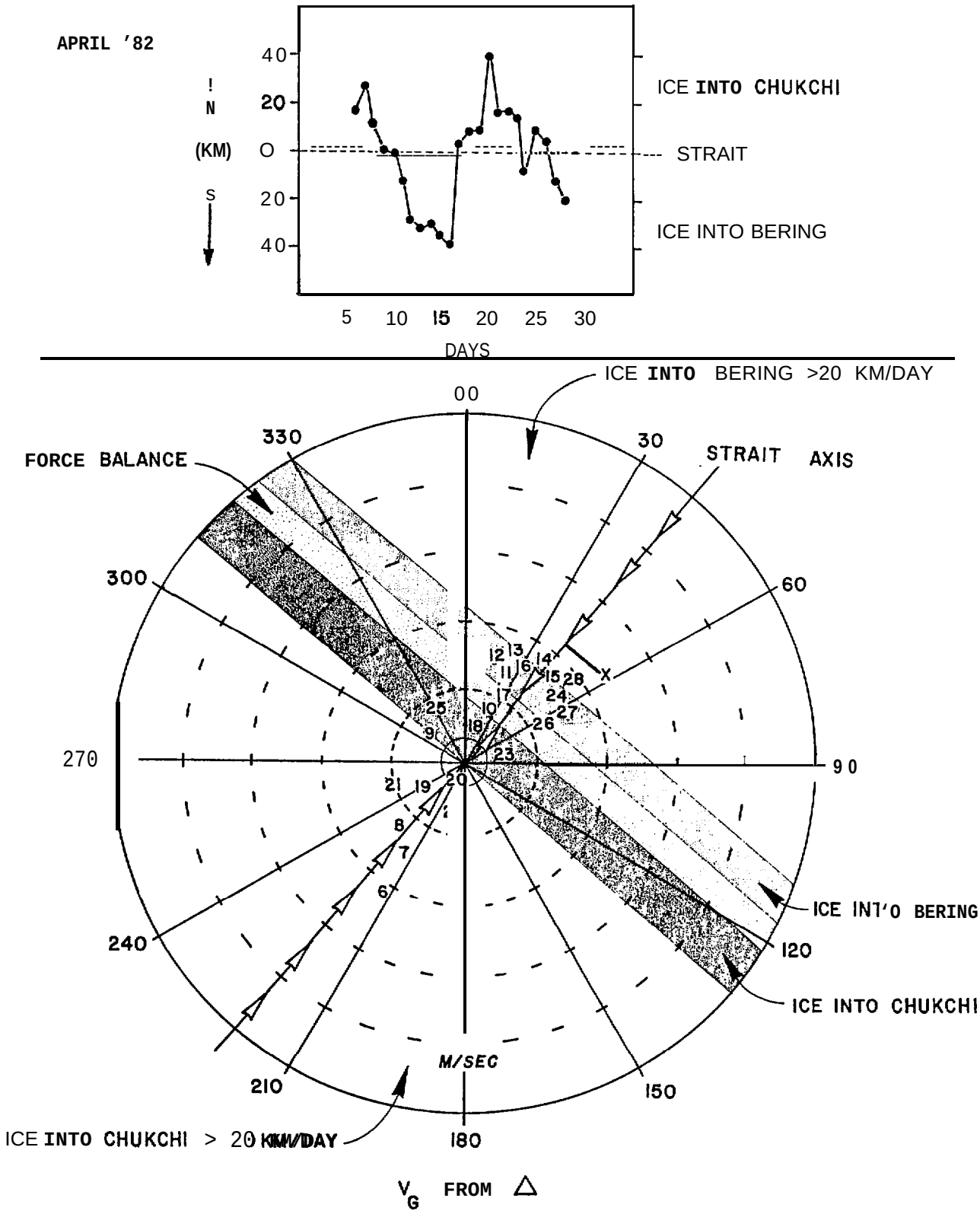

Fig. 9. Ice displacement (top) compared to MAPN V_G's for 6-28 April 1982 plotted with corresponding day numbers on the sea ice movement prediction nomogram (bottom). The number positions represent wind velocity vectors whose V_{40} components define the daily predicted ice movement zone. X is a sample V_G calculated from surface pressure data in Fig. 6. Drawing a perpendicular line from X to the Strait axis results in a V_{40} = 22 in^{s-}l. This is the Ice Into Bering > 20 km $(day)^{-1}$ Zone.

The first case was April 8, 1982 where > 20 km of northward movement was predicted but only 8 km measured. Possibly the unusually long string of previous days (17) with both recorded and predicted (by techniques from this study) northward sea ice movement resulted in minimal space for new ice advected into the Chukchi Sea.

The second case was April 12, 1982 where a V_G of 13.6 ins-l from 22.5° produced 31 km of actual ice movement to the south instead of < 20 km south predicted by the nomogram. Here the wind direction was 180° from the last major northward push (April 8, 1982) and only the second day of consisted V_G's from the northeast. There was evidently ample room for sea ice advection south through the Strait from the Chukchi Sea without need for additional deformation. It must be noted that these observed tendencies for diminished sea ice motion after 17 consecutive day of northward push (case 1) and enhanced sea ice motion after 180° wind direction reversals (case. 2) agree with the observations of Agerton and Kreider (1979). Their results for the Beaufort Sea have shown that the conditions for major sea ice movement are a wind speed threshold of 13 ms^{-1} and alternation of stress application direction by 180°.

The third case on April 19, 1982 had 10 km of net northward sea ice movement shown on the satellite imagery. The nomogram predicted movement >20 km to the north. There is no explanation for this discrepancy, however, the motion on the next day (April 20, 1982) was unusually large to the north, indicating that some compensating mechanism may be at work.

In summary, there were three bad predictions out of 23 or 87% correct. None of the “bad” predictions were off on the direction of ice movement, only the magnitude. The nomogram can be overlayed on polar coordinate graph paper and MAPN computed V_G's plotted very simply. The perpendicular to the V_{40} axis should give the predicted net sea ice movement.

(2) Buoy drift data (description from Reynolds and Pease, 1984)

Data buoys implanted on ice floes in the winter of 1982 were tracked by satellite through use of a position transponder called an ARGOS Data Acquisition Platform (ADAP), Model 901. These were made by Polar Research Laboratories in Santa Barbara, California. ARGOS is a cooperative project between Centre National d'Etudes Spatiales (CNES) of France, the U.S. National Aeronautics and Space Administration (NASA) and the National Oceanic and Atmospheric Administration (NOAA). The ARGOS receiving system is carried by NOAA polar orbiting satellites. Each ADAP platform position is received 8-12 times per day with an accuracy of 200 m in longitude and 100 m latitude. Table 3 presents the nomogram predictions versus various net buoy drift distances (Reynolds and Pease, 1984). The buoy locations chosen were between 1° south and .5° north of the Strait, because the MAPN grid is essentially south of the Strait proper (Fig. 1). The net movement of individual buoys on various ice floes is from a smaller data base and is not exactly the same as net ice movement taken from satellite photographs. However, future projects, using the high resolution all-weather capabilities of the buoys, might provide data for fine-tuning the nomogram technique. At least one buoy and sometimes three were in the"Strait area at various times from 3 February to 3 April 1982. In Table 3, net buoy displacement (X) to the north (N) or south (S) can be compared to the nomogram predictions (NP) for the given MAPN computed average velocities (V_G). There was agreement in 33 out of 40 days for 82.5% correct predictions. One case, February 12, 1982, had V_G change from 256°, 13 ins-l to 74°, 18 ms^{-1} in 12 hours which is a condition not included in the nomogram construction. On February 17, 18, and 27 and March 22 and 26, the predictions were off on net distance but not direction. The March 29 and 30 dates each had buoy movement (X) of 8 km north while the

TABLE 3

NET BUOY DISPLACEMENTS (X) VERSUS NOMOGRAM PREDICTIONS (NP)

Date (82)	Buoy #	x (km, N or S)	$\bar{V}_G$(direction)[("from], speed [in s^{-1}])	NP(km)	Agreement
3 Feb	2324	39N	139, 11	> 20N	yes
4 Feb	2324	39N	195, 11	> 20N	yes
5 Feb	2324	12N	112, 17 (sea ice moved westward also)	< 20N	yes
6 Feb	2320,2323, 2324	44N (Ave.)	226, 16	> 20N	yes
7 Feb	2320,2323 2324	72N (Ave.)	213, 16	> 20N	yes
8 Feb	2320,2323	66N (Ave.)	231, 9	> 20N	yes
9 Feb	2325	16N	320, 4	< 20N	yes
10 Feb	2325	10N	057, 7	< 20N	yes
11 Feb	2325	22N	011, 3 *(in 3 ms^{-1} zone consider ~ 0)	> 20N	yes*
12 Feb	2325	36N	(256, 13 to 74, 18 in 12 hrs)	no prediction	-
13 Feb	2325	10s	075, 16	< 20s	yes
14 Feb	2325	65S	021, 17	> 20s	yes
15 Feb	2323,2325	74S (Ave.)	017, 17	> 20s	yes
16 Feb	2320,2324	77S (Ave.)	025, 18	> 20s	yes
17 Feb	2320,2324	45S (Ave.)	037, 13	< 20s	no
18 Feb	2324	44s	024, 13	< 20s	no
"24 Feb	2320,2324	45N	205, 14	> 20N	yes
25 Feb	2320,2324	27N (Ave.)	195, 8	> 20N	yes
26 Feb	2320,2324	76N (Ave.)	193, 10	> 20N	yes
27 Feb	2324	12N	251, 6	> 20N	no

TABLE 3. (continued)

Date (82)	Buoy #	x (km, N or S)	$\bar{V}_G$(direction)[(°from], speed [ms^{-1})	NP(km)	Agreement
5 Mar	2325	36N	152, 11	> 20N	yes
6 Mar	2325	45N	125, 18	> 20N	yes
7 Mar	2325	45N	140, 15	> 20N	yes
8 Mar	2325	78N	137, 24	> 20N	yes
9 Mar	2325	65N	168, 13	> 20N	yes
19 Mar	2325	24S	057, 23	> 20s	yes
20 Mar	2325	51s	053, 29	> 20s	yes
21 Mar	2325	36S	062, 23	> 20s	yes
22 Mar	2325	8S	045, 21 *(P incresed ~ 8 mb in 12 hrs at all 3 stations)	> 20s	no*
23 Mar	2325	5N	339, 4 *(sea ice moved eastward also)	< 20N	yes*
24 Mar	2325	~3N	002, 8 *(mainly east motion)	force balance	yes*
25 Mar	2325	~3N	039, 8 *(some east motion)	force balance	yes*
26 Mar	2325	11N	135, 10 *(close to error bounds of MAPN)	> 20N	no*
27 Mar	2325	23N	133, 13	> 20N	yes
28 Mar	2325	22N	123, 5	> 20N	yes
29 Mar	2325	8N	049, 10 *(P increased ~ 5 mb in 12 hrs at all stations)	force balance	no*
30 Mar	2325	8N	036, 9	force balance	no
31 Mar	2325	~2N	062, 6	< 20N	yes
1 Apr	2325	7N	008, 6	< 20N	yes
2 Apr	2325	47N	163, 9	> 20N	yes
3 April	2325	36N	216, 16	> 20N	yes

nomogram predicted (NP) a force balance or O motion. The March 26 date showed X equal to 11 km north while NP was > 20 km north. In this last case, errors in the MAPN (Section 3) could have made the prediction incorrect.

The above mentioned cases on March 22 and 29, 1982 were probably not in geostrophic balance (l). Both showed the pressure field changing rapidly during the 00 to 1200 GMT time period at stations in the MAPN. Therefore, an additional wind velocity component proportional to the barometric tendencies directed from high to low tendency isopleths (isallobars) existed. The mathematical expression (5) for the wind component due to a changing pressure distribution, isallobaric component (VI), was derived in Brunt (1941):

$$V_I = \frac{-\nabla\dot{\rho}}{f^2\rho} \tag{5}$$

where all terms are defined as in (1) and (·) represents the partial derivative with respect to time. Using (5) the March 22, 1982, MAPN V_G (see Table 3) would have neglected an opposing V_I of ∿ 2 ms^{-1} from 145°. The March 29, 1982 MAPN V_G (see Table 3) would have an opposing V_I of ∿ 1.5 ms^{-1} from 227.

The same days also had maps showing isobars with the radius of curvature less than 300 km (see Kozo 1982). This type of wind flow, called gradient flow, requires that centrifugal force be added to the terms in (1) for a force balance. The March 22 and 29 dates were instances of cyclonic flow making V_G an overestimate of the true free stream wind velocity (VT). The expression (6) for VT is (Holton, 1973):

$$\frac{V_T^2}{R} + fV_T - fV_G = 0 \tag{6}$$

where R ≡ radius of curvature of the isobars. Using (6), the March 22 VT is 15.9 ms^{-1} from 45° which if used in the nomogram would give a correct prediction of < 20 km S (see Table 2). The March 19 VT is 8.5 ins-l from 049°

which combined with V_I above gives a correct prediction of < 20 km N within the MAPN error bounds.

The present MAPN does not account for isallobaric effects or gradient flow since a simple procedure for prediction was examined first. These extra refinements can be built into the wind velocity calculation and on application to the nomogram will increase the accuracy ∿ 5%.

g. Discovery of solid double sea ice arches

The double sea ice arch represents the longer duration second mode of ice immobilization mentioned in Section 4d. This mode is rare in the Bering Strait since only five cases have been seen on inspection of 11 years of sea ice satellite data. A satellite photograph (Fig. 10) taken May 5, 1980 shows the characteristic solid double ice arch in the Strait using the tip of the Chukchi Peninsula (Cape Dezhneva), the Diomede Islands and the Seward Peninsula tip (Cape Wales) as anchor points. Norton Sound is totally free of ice (see Fig.2 for possible mechanism of ice removal) except for shore-fast sea ice on the southern side. Also, there is a large expanse of open water south of the Bering Strait arches and south of St. Lawrence Island. Since the image was taken 21 days after the arches formed, it appears that it was not cold enough for new ice formation and the presence of arches prevented resupply by old ice advection south into the Bering. These arches are not the arched fractures seen in sea ice during failure modes (Sodhi, 1977; Reimer et al., 1979), but evidently represent strong impediments to sea ice movement to the south. As evidence of the lack of fractures in the ice canopy during the solid arch phase, the above (April 14 to May 10, 1980) period represented a halt in Bowhead whale migration through the Strait (Hufford, 1984; National Weather Service, Anchorage, pers comm.).

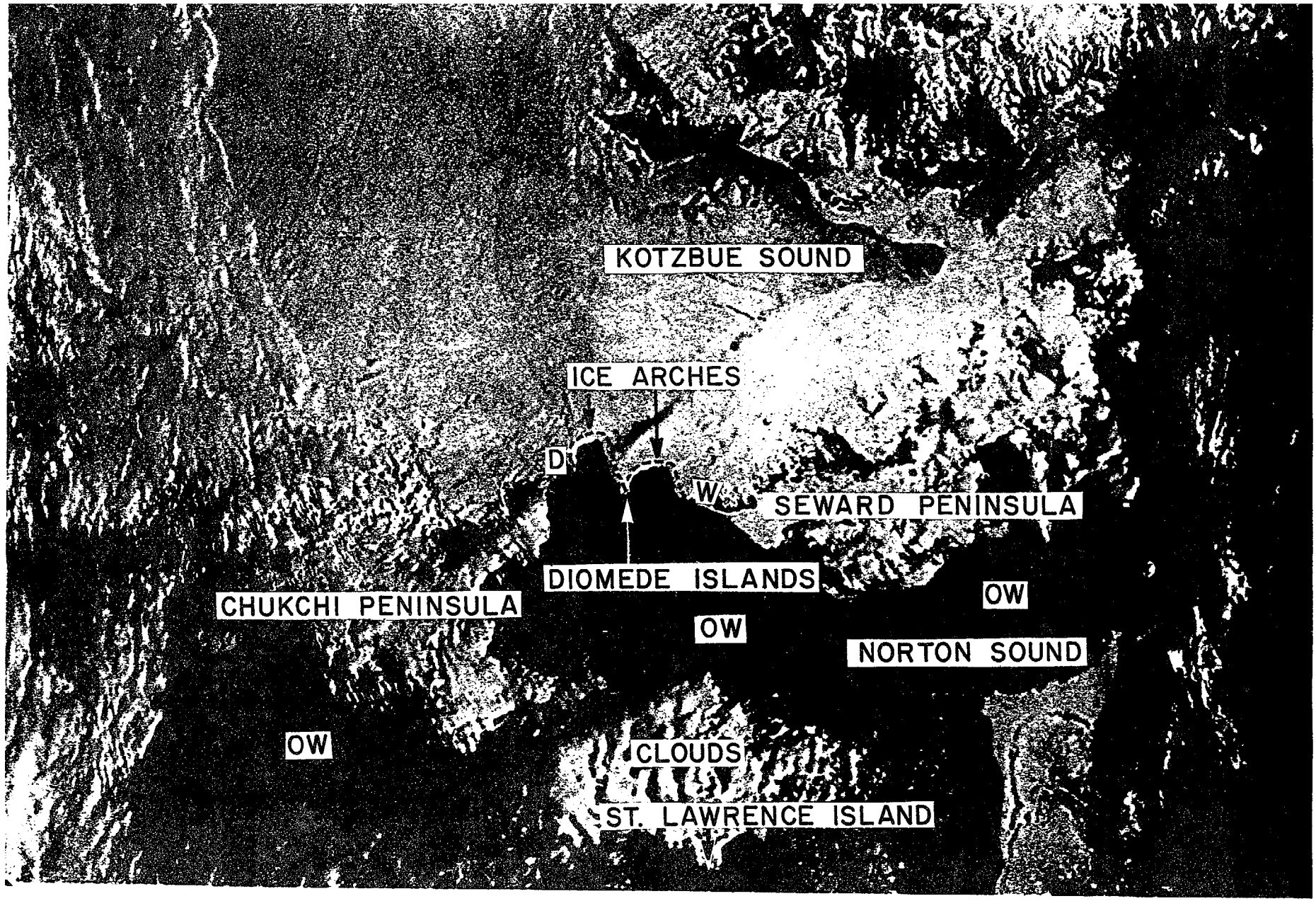

Fig. 10. A photograph made from a satellite image taken May 5, 1980 showing the characteristic solid double ice arch in the Bering Strait using the tip of the Chukchi Peninsula (D), the Diomede Islands and the Seward Peninsula (W) tip as anchor points. There is a large expanse of open water (OW) south of the Strait,

The double arches were discovered indirectly through failure of the nomogram prediction system. In all double arch cases, the nomogram with $\bar{V}_G$ from the MAPN predicted > 20 km $(day)^{-1}$ of net ice movement into the Bering for at least 50% of the arch period. In addition, the > 20 mb pressure difference ice breakout criterion (Reimer et al., 1979) from Cape Schmidt to Nome (Fig. 1, Section 1) was exceeded at some time during all the double arch periods. This criterion represents τ_{40} of 13.5 $m\,s^{-1}$ for an air density of 1.4 kg m^{-3} which would produce a < 20 km $(day)^{-1}$ sea ice movement south through the Strait according to the nomogram. Fig. 11 shows sample MAPN V_G's from designated periods such as April 14-May 10, 1980, February 26-March 8, 1984, and March 22-April 21, 1984 plotted on the nomogram. There were several cases with $\tau_{40} \sim 26$ s^{-1} and no ice movement at all through the Strait, though movement could be seen above and below.

The theory predicting the limiting spans for arching of granular material flowing through a chute (Gardner, 1962; Richmond and Gardner 1962) as adapted by Sodhi (1977) will be used to show the reason for double arch" existence despite the strong MAPN winds seen in Fig. 11. It seems possible that the double arches are a natural phenomenon resulting from a persistent period of strong wind velocities which most certainly would destroy a single arch across the entire Strait. Fig. 12 is a blow-up of the Strait area from Fig. 10 with the Chukchi and Seward Peninsulas and the Diomede Islands again shown as anchor points for the sea ice. The dashed curves differentiate the sea ice arches from the coastal boundaries and the dark areas are open water. The strength of a single arch can be estimated by comparing the arches in Fig. 12 to the inset drawing. The span width (2A) of the arch from the Diomede Islands to Seward Peninsula is 41 km and from the Chukchi Peninsula to the Diomedes is 37 km. The width of the Diomede Island blockage zone (see

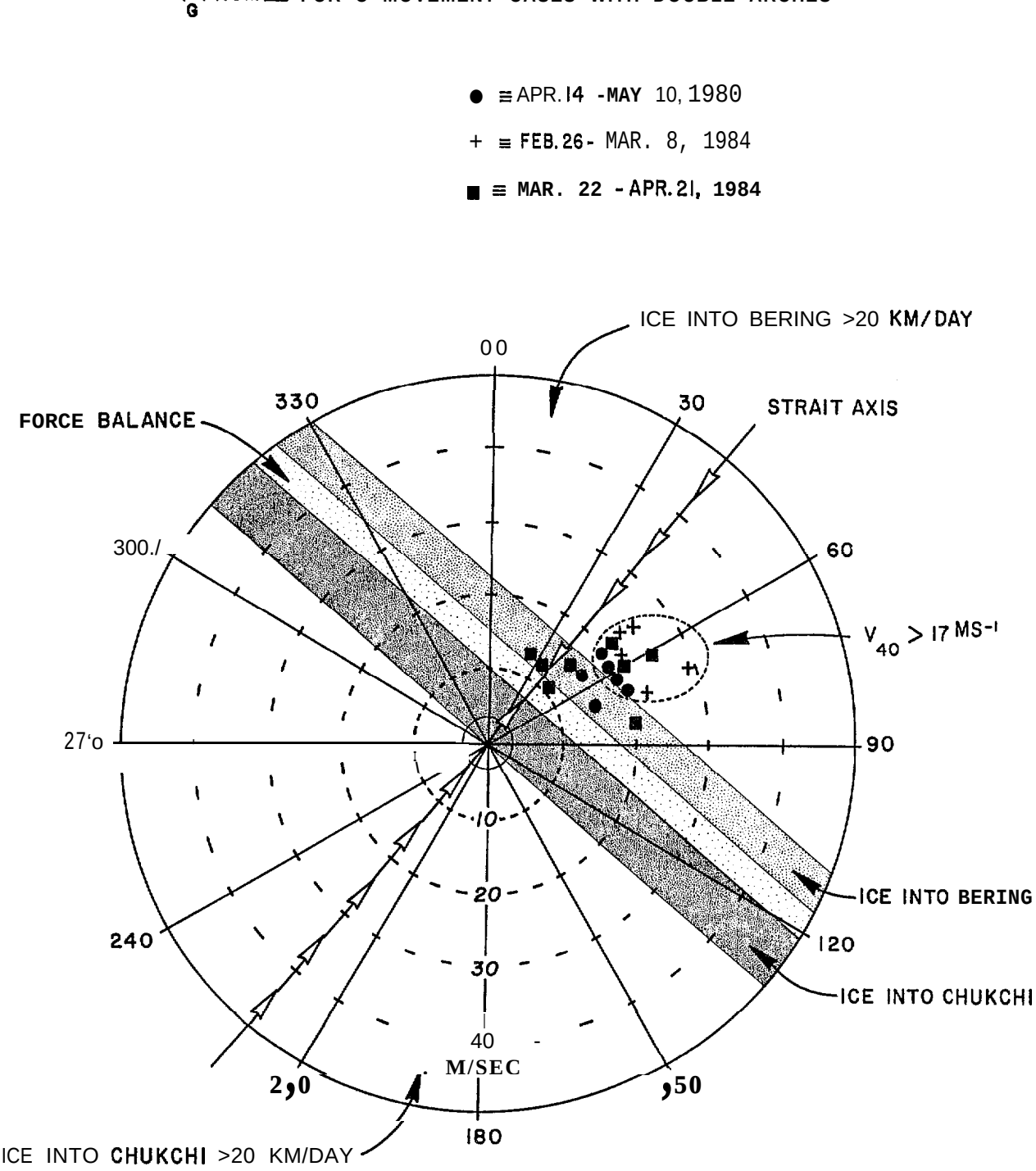

'ig. 11. Samples of MAPN V_G' s from designated double arch periods April 14-May 10, 1980, February 26-March 8, 1984, and March 22-April 21, 1984 plotted on the nomogram. There are several cases (enclosed by dashed oval) with $V_{40} \geqq 17$ ms^{-1} indicating a predicted ice movement into the Bering Sea of greater than 20 km(day)$^{-1}$.

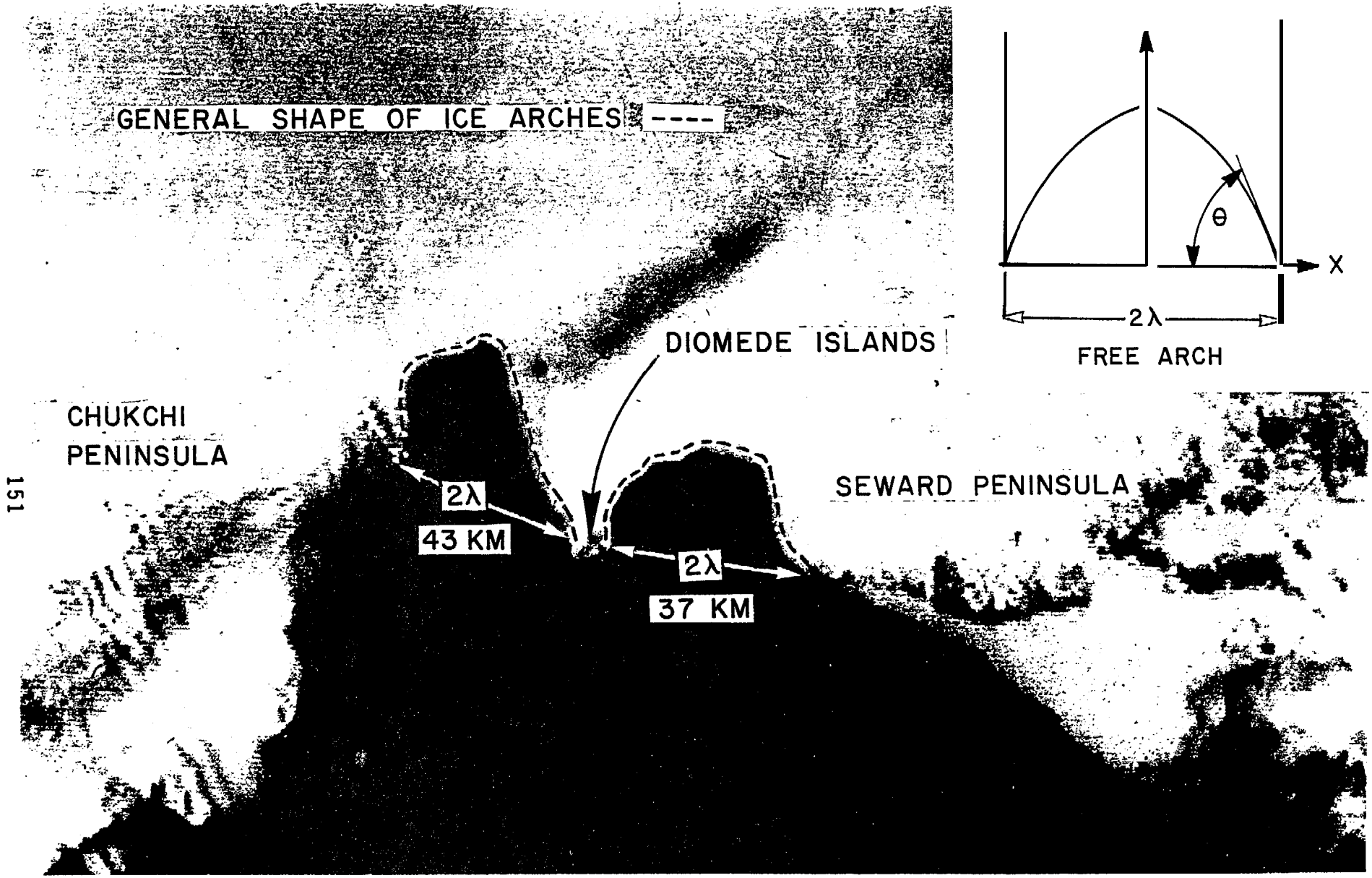

Fig. 12. An enlargement of the Strait area taken from the Fig. 10 photograph. The dashed curves show the actual sea ice arches to avoid confusion with land boundaries. The dark area is open water. The inset (top) is a sketch of an idealized free arch showing the span width (2A) and the angle (θ) between the horizontal and tangent to the free surface.

Shapiro and Burns, 1975a) is 7 km. Θ can be read with a compass from Fig. 12. The eastern arch (Diomede Islands-Seward Peninsula) has a $\Theta \sim 80°$ while the western arch (Diomede Islands-Chukchi Peninsula) is more irregular with an average Θ of $\sim 80°$ also. From (7)

$$\Theta = \Pi/4 + \phi/2 \tag{7}$$

where $\phi \equiv$ angle of internal friction

$\Theta \equiv$ angle between the horizontal and tangent to the arch profile

ϕ is estimated as 70° for both arches. Next (8) is used to solve for τ as defined by (9).

$$\lambda = \frac{c}{\tau}(1 + \sin \phi) \tag{8}$$

$$\tau = p\, CV^2 \tag{9}$$

Here:

$\lambda \equiv$ half span width (m)

$c \equiv$ cohesive strength (Nm^{-1})

$\tau \equiv$ net stress per unit area (Nm^{-2})
(wind and water stress combined)

$\rho \equiv$ mass density of medium (kg m^{-3})

$C \equiv$ drag coefficient (unitless)

$V \equiv$ wind velocity (ms^{-1})

Cohesive strength (c) for Amundsen Channel (Beaufort Sea, June) sea ice in a solid arch was estimated from (8) and (9) at failure to be 1993 nm^{-1} (Sodhi, 1977). The net stress (τ) applied to this arch (0 water stress assumed) was calculated using a typical 10 m air-ice drag coefficient of $1X10^{-3}$ for C and local winds for V. Recent Bering Sea work by Walter et al.

(1984) shows the drag coefficient to be $3x10^{-3}$ or three times the Sodhi (1977) estimate. Using this newer value for C would give c = 5979 Nm^{-1} as the cohesive strength of sea ice at failure. Given this c, taking $\phi = 70°$, and A ~ $20x10^{3}$ m (double arches) and substituting into (8), τ (net) = .58 . Nm^{-2}.

Remembering that water stress generally opposes wind stress from the north, τ_w is defined by (3) in Section 4d and estimated to be -.16 Nm^{2}. The net stress τ, as seen in (10), will allow calculation of air stress τ_a (defined by [4] , Section 4d) .

$$\tau = \tau_a + \tau_w \qquad (10)$$

Therefore $\tau_a = (.58) - (-.16) = .74\ Nm^{-2}$.

Hence from (3)

$$U_a^2 = \frac{\tau_a}{pa\ C_a\ r_a^2} = \frac{.74}{1.3x3x10^{-3}x(.6)^2}$$

or $U_a = 23\ ms^{-1} = ,_{40}$ on nomogram axis.

This geostrophic wind corresponds to a surface wind of 13.8 ms^{-1} . Surface winds of this magnitude from November through May occur less than 10% of the time (Brewer et al., 1977) at Tin City (near Cape Wales, Fig. 1) which is close to the Strait. 'he estimated ,40 value 'f 23 's $^{-1}$ is similar to the maximum ,40 seen on Fig. 11 which is approximately 26 ms^{-1}. The cohesive strength estimate used here could have been slightly larger since no evidence of arch breakup during these winds existed. The actual way that the arches are finally destroyed is a relaxation of the northerly winds and a switch to pure water stress or wind and water stress combined from the south. It should be noted that using the half span length for a single arch across the entire Strait (~ 42.5 km) in (8) with all other parameters the same yields τ = .27

Insertion into (10) gives a V_{40} = 17.5 ms^{-1} which would be exceeded by 50% of the values shown in Fig. 11, thereby leading to arch failure.

5. Summary and conclusions

The combination of MAPN calculated V_G's and the polar coordinate nomogram provides an all weather sea ice movement nowcasting capability for the Bering Strait with an average accuracy of 85% . The MAPN improvement over NMC surface pressure analyses and pattern recognition techniques has been demonstrated. This study, though meteorologically oriented, also has shed further light on both sea ice and oceanographic phenomena. The ocean currents, in particular, in the Strait area are crucial to the prediction s theme.

a. Sea ice movement modes

Three modes of ice movement were found. The first is a southward movement into the Bering Sea requiring a $V_{40} \geq 12$ in s-1. The second mode is movement into the Chukchi Sea during weak synoptic winds, driven by a north flowing ocean current made up of tidal and baroclinic residuals. The third mode is northward ice movement under the combined influence of winds from the southwest and a pre-existing north flowing ocean current.

b Sea ice immobilization modes

There were two modes of ice immobilization found in the Strait. The first mode is an apparent balance between wind stress from the north and a water stress provided by a current from the south. Internal ice stresses and fast-ice boundary orientation must play a role, but they are not covered in

this study. The 0 net movement is short term, usually lasting less than one week. The second mode was discovered only five times in 11 years. In each case, the polar coordinate nomogram predicted large ice movement south through the Strait when, in fact, there was none. Double solid sea ice arches made possible by the Diomede Islands anchoring the middle column of the arches were seen as the culprits. A theoretical calculation of the strength of single arches across the entire Bering Strait showed fracturing at the MAPN generated V_G's. However, the same calculation on double arches showed the ability to withstand the V_G's ($V_{40} \sim 26$ ms^{-1}) generated during the arch periods. This longer period immobilization mode (up to three weeks) can hinder spring whale migration into the Chukchi and aid in opening up the region below the Strait as well as Norton Sound.

c. Driving force behind the north flowing current in the Strait

The general higher sea level in the Bering over that of the Arctic Ocean and the compensatory circulations caused by local sea level differences after northeasterly winds can create northward flowing ocean currents through the Bering Straight without apparent local wind pushing. However, through the course of this study, several northward ice flow movement events were seen without apparent wind forcing or large scale atmospheric pressure fields conducive to raising the sea level in the Bering over that of the Arctic Ocean (Chukchi). Also, northward ice movement continued three days beyond relaxation of strong northeasterly winds, precluding compensatory circulations due to local sea level differences. Work by investigators mentioned above, plus evidence presented, points to residual northward transport from the tide and ocean density fields.

d. Recommendations for future work

The MAPN-nomogram technique can be improved in several respects if a need arises. Bad prediction can often be traced to two major cases where a geostrophic balance does not exist. One case is under accelerating conditions when pressure is changing rapidly requiring an isallobaric component of the wind. Another case is when strong curvature of the isobars exists (radius of curvature less than 300 km), implying that a gradient wind balance is needed. The nomogram itself can be finer tuned if more data of the type collected by Reynolds and Pease (1984) can be matched to satellite information. This data might prove very useful to determine further differences in northward ice movement driven by a wind and current push versus movement driven by a current alone. The MAPN accuracy can be improved by a cooperative visitation program involving the Russian sites in the network. A barometric standard could be used to calibrate all three sites to arrive at more precise Vp values from which V_G is calculated.

Acknowledgments. The investigator would like to credit the extensive work by Dr. William J. Stringer and Ms. Lenora J. Wattum of the Geophysical Institute at the University of Alaska, without whose efforts this report would not be possible. This project was funded by the Minerals Management Service, U. S. Department of the Interior, through interagency agreement with the National Oceanic and Atmospheric Administration, U. S. Department of Commerce, as part of the Outer Continental Shelf Environmental Assessment Program.

REFERENCES

Agerton, D. J. and J. R. Kreider, 1979: Correlation of storms and major ice movements in the nearshore Alaska Beaufort Sea. Fifth International Conference on Port and Ocean Engineering under Arctic Conditions. Norwegian Institute of Technology, 1,177-189.

Albright, M., 1980: Geostrophic wind calculations for AIDJEX, in A Symposium on Sea Ice Processes and Models. Proc. International Commission on Snow and Ice/Arctic Ice Dynamics Joint Experiment (cd. by Robert S. Pritchard), University of Washington Press, Seattle, 402-409.

Brewer, W. A., H. F. Diaz, A. S. Prechtel, H. W. Searby and J. L. Wise, 1977: Climatic Atlas of the Outer Continental Shelf Waters and Coastal Regions of Alaska. NOAA, NCC, EDS, Asheville, 409 pp.

Browning, K. A., 1982: Preface in Nowcasting (cd. by K. A. Browning). Academic Press, New York, IX-XI.

Brunt, D., 1941: Physical and Dynamical Meteorology. Cambridge University Press, London, 428 pp.

Coachman, L. K. and K. Aagaard, 1981: Reevaluation of water transports in the vicinity of Bering Strait, Chapter 7 in The Eastern Bering Sea Shelf: Oceanography and Resources (cd. by D. W. Hood and J. A. Calder), University of Washington Press, Seattle, 95-110.

Coachman, L. K., K. Aagaard and R. B. Tripp, 1975: Bering Strait: The Regional Physical Oceanography. University of Washington Press, Seattle and London, 172 pp.

Dickey, W. W., 1961: A study of a topographic effect on wind in the arctic. J. Meteor. , 18, 790-803.

Drury, W. H., C. Ramsdell, J. B. French, Jr. , 1981: Ecological studies in the Bering Strait region. Environmental assessment of the Alaska Continental shelf. NOAA/OCSEAP Final Rpt. Bio. Studies, 11,175-487.

Gardner, G. C., 1962: Limiting conditions for flow of a cohesive granular material down an inclined plane (chute) or between parallel inclined walls (bin or channel). Chem. Eng. Sci., 17,107-1086.

Holton, J. R., 1972: An Introduction to Dynamic Meteorology. Academic Press, New York, 319 pp.

Hufford, G. and R. Scheidt, 1984: Interaction of Norton Sound Ice and Weather, Abs. in 1984 Arctic Science Conference (35th Alaskan Conference), Oct. 2-5, 1984, Anchorage, Alaska, sponsored by Amer. Ass. for Adv. of Sci.-Arctic Div., Amer. Met. Sot. and Arctic Inst. of North America, 109 pp.

Kovacs, A. and D. S. Sodhi, 1981: Sea ice piling at Fairway Rock, Bering Strait, Alaska: Observations and theoretical analyses. Proc. Sixth Int. Conf. on Port and Ocean Eng. under Arctic Cond. POAC-81, Quebec, Canada, 2,985-999.

Kozo, T. L., 1984: Mesoscale wind phenomena along the Alaska Beaufort Sea Coast, in The Alaska Beaufort Sea: Ecosystems and Environment (cd. by P. W. Barnes, D. M. Schell and E. Reimnitz). Academic Press, New York, pp. 23-45.

—, 1982: An observational study of sea breezes along the Alaska Beaufort Sea Coast: Part I. J. App. Meteor. , 12, 891-905.

—-----, 1980: Mountain barrier baroclinity effects on surface winds along the Alaskan Arctic Coast. Geophysical Research Letters, 7,377-380.

— and W. B. Tucker, 1974: Sea ice bottomside features in the Denmark Strait. J. Geophys. Res., 79, 4505-4511.

Liu, S. K. and J. J. Leenderste, 1984: Modeling the Alaskan coastal waters, in Three-dimensional Shelf Models (cd. by N. Heaps), Amer. Geophys Union, Washington, D. C., in press.

Pease, C. H. and J. E. Overland, 1984: An atmospherically driven sea-ice drift model for the Bering Sea. Ann. Glaciol., 5, 111-113.

Ray, V. M. and W. R. Dupre, 1981: The ice-dominated regimen of Norton Sound and adjacent areas of the Bering Sea. Chapter 16 in The Eastern Bering Sea Shelf: Oceanography and Resources (cd. by D. W. Hood and J. A. Calder). University of Washington Press, Seattle, pp. 263-178.

Reimer, R. W., R. S. Pritchard and M. D. Coon, 1979: Beaufort and Chukchi Sea ice motion: Part 2. Onset of large scale Chukchi Sea ice breakout, Elow Res. Rpt. No. 133, Kent, Washington, 92 pp.

Reynolds, M. and C. H. Pease, 1984: Drift characteristics of the northeastern Bering sea ice during 1982. NOAA Tech. Memo. ERL-PMEL-55, Seattle, Washington, 135 pp.

Richmond, O. and G. C. Gardner, 1962: Limiting spans for arching of bulk material in vertical channels. Chem. Eng. Sci., 17, 1071-1078.

Shapiro, L. H. and J. J. Burns, 1975a: Major late-winter features of ice in Northern Bering and Chukchi Seas as determined from satellite imagery. Geophysical Inst. Rpt. No UAG R-236, Sea Grant Rpt. No. 75-8, University of Alaska, Fairbanks, 14 pp.

Shapiro, L. H. and J. J. Burns, 1975b: Satellite observations of sea ice movement in the Bering Strait region. In Climate of the Arctic, University of Alaska, Fairbanks, pp. 379-386.

Sodhi, D. S., 1977: Ice arching and the drift of pack ice through restricted channels. Cold Regions Research and Engineering Laboratory, CRREL Rpt. 77-18, Hanover, New Hampshire, 11 pp.

Stringer, W. J. and G. L. Hufford, 1982: Interaction of Bering Sea and Norton Sound pack ice. Arctic and Alpine Res., 14,149-156.

Walter, B. A., J. E. Overland and R.. O. Gilmer, 1984: Air-ice drag coefficients for first-year sea ice derived from aircraft measurements. J. Geophys. Res., 89, 6525-6531.